X-625-71-308
PREPRINT

ELECTRON AND POSITIVE ION DENSITY ALTITUDE DISTRIBUTIONS IN THE EQUATORIAL D REGION

A. C. AIKIN
R. A. GOLDBERG
Y. V. SOMAYAJULU

AUGUST 1971

GSFC
GODDARD SPACE FLIGHT CENTER
GREENBELT, MARYLAND

ELECTRON AND POSITIVE ION DENSITY ALTITUDE DISTRIBUTIONS IN THE EQUATORIAL D REGION

by

A. C. Aikin
R. A. Goldberg
Laboratory for Planetary Atmospheres
NASA/Goddard Space Flight Center
Greenbelt, Maryland

and

Y. V. Somayajulu
National Physical Laboratory
New Delhi, India

ABSTRACT

Three simultaneous rocket measurements of D region ionization sources and electron and ion densities have been made in one day. Electron density profiles for solar zenith angles of 53.2, 27.8 and 48.3^{o} are displayed. The profiles are found to be quite similar to those reported for mid-latitudes under quiet conditions. Using simultaneous measurement of the X-ray flux together with NO ionization estimates based on recent measurements of NO by Meira (1971) and $O_2(^1\Delta_g)$ ionization rates by Huffman et al (1971), the ion pair production function is computed. It is demonstrated that the charged particle distribution can be explained using this production function and an effective recombination coefficient compatible with recent laboratory measurements of the dissociative recombination coefficient for electrons with hydrated cluster ions.

INTRODUCTION

The D region is the least understood part of the ionosphere. Although several sources of ionization have been proposed, uncertainties of measurement have led to wide speculation concerning their relative importance. Latitudinal, seasonal, and diurnal behavior of the most easily measured parameter, the electron density, are ill-defined. The species of ions present are either unknown or at best known only qualitatively. It is therefore, necessary to improve measuring techniques and to conduct experiments in which the sources of ionization, the resultant electron and ion density distribution, and the species of ion are all determined simultaneously.

Three Nike-Apache rockets were launched from the Thumba Equatorial Rocket Range in India, near the geomagnetic equator, on March 19, 1970. The instrumentation on each rocket together with the local time of launch and solar zenith angle are listed in Table 1. Additional details relating to the flight and the ion composition measurements are dealt with in Goldberg and Aikin (1971). The present paper is concerned with the electron and positive ion densities and their relationship to the different sources of ionization. A production function is derived and used in conjunction with the charged particle density to evaluate the effective recombination coefficient, α.

ELECTRON DENSITY EXPERIMENT

The electron density distribution has been determined from a radio wave absorption experiment developed by Kane

(1969). The output of a CW transmitter is alternately fed to antennas oriented magnetic east-west (ordinary mode) and north-south (extraordinary mode). The amplitudes of the resulting signals are monitored by a rocket-borne receiver with a linearly polarized antenna.

The azimuth of the rocket trajectories nearly coincided with magnetic west to permit radio wave transmission quasi-transverse to the Earth's magnetic field. The frequencies 3030 and 1865 KHz were chosen for the experiment on each of the three payloads. The switching of the propagation mode was accomplished every 0.5 seconds or approximately once each 2.5 to 4 rolls of the payload. Figures 1a, 1b. and 1c give the resultant profiles together with their respective scatter of data points for the extraordinary wave mode on each of the three payloads. Ordinary wave data contain more scatter than extraordinary and appear to be less accurate. All data were reduced using total absorption rather than differential absorption techniques for increased accuracy in the results.

ION DENSITY PROFILES

Total positive ion density was measured in situ using the Gerdien condenser technique described by Bourdeau et al., (1966). A schematic of the instrument used in the present experiments is shown in Figure 2. On both flights 14.425 and 14.424, the Gerdien was operated with the collector (B) at a fixed D.C. bias of -4 volts with respect to the grounded

payload housing. Assuming total current collection for the flow passing through the instrument, the ion density profile obtained for 14.424 is illustrated in Figure 1b. Above 75 km there is excellent agreement between the positive ion and electron density. There is an increasing deviation between the two profiles below 70 km which is attributed to the presence of negative ions. However, the exact concentration of these negative ions cannot be determined because of inaccuracies which may exist in the radio absorption data and the Gerdien flow.

The positive ion density data for rocket 14.425 was not in good quantative agreement with the electron density profile and it was necessary to normalize the data to the electron density profile shown in Figure 1a by shifting it as indicated. The deviation between Gerdien and radio absorption data on this flight is believed to be primarily due to Gerdien data interpretation. This is caused by oblique shock effects which pinch off the effective flow cross-section, i.e. effective aperture area, leading to erroneously small positive ion densities. Also, NASA 14.425 traveled at a velocity of Mach 2.2 in the region of discrepancy, whereas the better agreement of 14.424 occurred at Mach 3.2. These differences and their effects on pinching the flow are currently under investigation.

QUALITATIVE RESULTS

The data discussed in the previous two sections have been combined to form the three profiles for electron

density shown in Figure 3. These data were taken under quiet time conditions with Ap = 5.

The profiles exhibit the shape characteristics of the lower ionosphere at midlatitudes. There is a Chapman like D region centered between 75 and 85 km. Above 85 km there is a steep gradient of electron density which characterizes the bottom of the E region.

The most interesting aspects of the profiles are the changes which occur with solar zenith angle (χ). The E region is seen to shift downward for small values of χ. Solar control of the D region extends to 70 km which, as we shall see in a future section, is indicative of large concentrations of nitric oxide. The peak density of the D region resembles that of midlatitudes under quiet solar conditions. There is also an electron density minimum in the vicinity of the mesopause. This has been observed at midlatitudes and attributed to electron attachment to dust (Aikin et al., 1964).

One interesting aspect of the comparison between pro files is the possible existence of a diurnal asymmetry, although this observation may be somewhat marginal within the accuracies estimated for the experiment. There is apparently a much larger change between $\chi = 53^{o}$ and 28^{o} than between $\chi = 28^{o}$ and 48^{o} below 100 km. The measurement for $\chi = 48^{o}$ occurred in the afternoon while the remaining two occurred in the morning. This asymmetry was also observed in medium frequency absorption measurements taken

during the day of the rocket flights at Colombo, Ceylon (Gnanalingam, private communication). Similar ground-based observations have been reported previously (Rao et al., 1962; Haug et al., 1970).

SOLAR X-RAY PROPORTIONAL COUNTER EXPERIMENT

Included in the payloads of rockets 14.425 and 14.372 were X-ray proportional counters. The experiment consisted of an LND side window proportional counter tube whose gas filling was xenon plus 10% CH_4 at 760 $\pm$ 5 mm Hg. Each window diameter was 2.54 cm; the window material was beryllium of 2.54×10^{-2}cm thickness for 14.425 and 5.08×10^{-2}cm for 14.372.

The output of the proportional counter is fed into a charge sensitive amplifier, the output of which consists of pulses in the range 0 - 5 v dc. These pulses are stretched to a duration of 200 μ sec with a rise and fall time of 20 μ sec. Recovery time from the termination of the stretched pulse for a pulse of mean pulse height to 5% of the mean pulse height is 150μ sec. The resulting stretched pulses are telemetered to the ground over a 5 KHz bandwidth telemetry channel. A pulse rate counter is included which telemeters a 0 - 5 volt signal that is proportional to the logarithm of the pulse repetition frequency.

The unattenuated X-ray spectra obtained from the two payloads are shown in Figure 4. They compare favorably with Solrad 9 satellite ion chamber results below 5A. Kreplin

(private communication) has indicated the 1A to 8A integrated flux values for the local times of 14.425, 14.424 and 14.372 to be 1×10^{-3}, 1.3×10^{-3} and 9.0×10^{-4} ergs/cm^2 sec, respectively. Kreplin (1961) has outlined the procedure for obtaining integrated flux from satellite X-ray ion chamber measurements such as those made on Solrad 9. Between 3 and 8A, a 2×10^6 ^oK gray body is assumed while below 3A, a 10^7 ^oK gray body is used. In each case an appropriate dillution factor is chosen. For comparison purposes two gray body curves are shown in Figure 4. Gray body I corresponds to a temperature of 2×10^6 ^oK and a dillution factor of 5×10^{-15}. The integrated flux is 1.7×10^{-3} ergs/cm^2 sec. Gray body II represents a temperature of 10^7 ^oK and a dillution factor of 1×10^{-21}. The integrated flux below 3A is 2.5×10^{-6} ergs/cm^2 sec, well below the threshold of 1×10^{-5} ergs/cm^2 sec for the satellite 0.5 - 3A ion chamber. The proportional counter results are illustrated in Figure 4 and are seen to concur with the spectra estimated from Solrad 9 data.

PRODUCTION FUNCTION

In the absence of solar X-ray flares and energetic particle precipitation, the primary D region ionization source is solar Lyman alpha radiation acting on nitric oxide. Unfortunately the nitric oxide distribution has been one of the principal uncertainties in explaining the D region. Theoretical NO concentrations derived from photochemical equilibrium involving the reaction of ground

state nitrogen atoms with oxygen and nitric oxide are not large enough to account for the required ion-pair production function, Aikin et al. (1964). On the other hand NO distributions derived from rocket measurements of resonance fluorescence of nitric oxide gamma bands (Pearce, 1969) would require drastic restructuring of the theory of electron loss processes and be inconsistent with observations of solar flare X-ray enhancements of D region ionization, (Somayajulu and Aikin, 1968). However, recent observations of Meira (1971) have shown that in the D region the analysis of previous nitric oxide resonance fluorescence data did not consider the background due to Rayleigh scattering and so overestimated the nitric oxide concentration.

Two similar rocket-borne spectrophotometer measurements were made by Meira at Wallops Island, Virginia in January, 1969. The range of measured nitric oxide values is shown in Figure 5. An ion pair production function has been derived to correspond to the solar zenith angle for each rocket flight. It employs an NO mixing distribution passing through the lower limit of the error estimate of the best fit of Meira's data. This value is further justified by the recent results of Rusch and Barth (1971) who have discovered a trend toward lower values of NO in the equatorial region. The resulting production function, $q(NO)$, for $\chi = 28^{o}$ is shown in Figure 6.

An X-ray production function based on the rocket proportional counter spectra and satellite results is also

shown in Figure 6. Due to the hardness of the spectrum, X-rays are not a negligible contribution to the D region ionization rate and with cosmic rays constitute the major source for ionization of the major atmospheric constituents. The expression for the contribution due to cosmic rays is

$$q = q_o \, n(z)/n_o$$

where q_o is ion pair production function under standard conditions at the geomagnetic equator, i.e. 25 ion pairs/cm^3sec (Nicolet and Aikin, 1960). The number of particles in a standard atmosphere n_o, is 2.7×10^{19} cm^{-3}. The resulting cosmic ray production function is also shown in Figure 6 and merges with the X-ray ionization rate.

It has been suggested by Hunten and McElroy (1968) that photoionization of $O_2(^1\Delta_g)$ at $\lambda < 1118$ Å is an important source of D region ionization. Huffman et al. (1971) have pointed out that this would indeed be the case if there were no CO_2 in the mesosphere. Including the expected atmospheric CO_2 absorption of the ionizing radiation leads to the ion pair production function shown in Figure 6. This is consistent with Huffmann's conclusions. The ionization of $O_2(^1\Delta_g)$ is therefore, not a significant source of D region ionization. If anything it plays a minor role in the formation of the E region.

The possibility that O_2 can be raised to vibrationally excited states and subsequently ionized as suggested by Inn (1961, a, b) can also be discarded. It has been shown

by Hudson (1971) that such a sequence will lead to dissociation of the O_2 molecule rather than ionization.

The sources of ionization for the equatorial D region have been reviewed and estimated. We conclude that sources listed by Nicolet and Aikin (1960), i.e. ionization of nitric oxide by solar Lyman alpha, short wavelength solar X-rays and galactic cosmic rays, and a small contribution due to $O_2(^1\Delta_g)$ ionization, are of primary importance for describing the D region ionosphere under quiet conditions.

EFFECTIVE RECOMBINATION COEFFICIENT

The term "effective recombination coefficient" is used here to define the ratio, $\alpha = \sum_i q_i/N_e^2$ where q_i is the ion production rate for each ion species "i" and N_e is the electron density. It is a useful parameter because it tells one if the chosen ion-pair production function is consistent with current ideas on the magnitude of the loss rate.

The α's which are derived from the ion pair production functions and the electron density profiles at $\chi = 28^o$ are shown in Figure 7 for two nitric oxide distributions at the lower and upper limits of Meira's NO measurement. Similar results are obtained for $\chi = 53^o$ and 48^o. They are quite significant when compared with recent measurements of Biondi (private communication) for the dissociative recombination coefficients of the water clusters ions 19^+,

H_3O^+; 37^+, $H_3O^+ \cdot (H_2O)$; and 55^+, $H_3O^+ \cdot (H_2O)_2$. Measurements at 300 ^oK are modified by the term $(300/T)^{3/2}$ so that

$$\alpha_{19^+} = 1.3 \times 10^{-6} \left(\frac{300}{T}\right)^{3/2}$$

$$\alpha_{37^+} = 2.7 \times 10^{-6} \left(\frac{300}{T}\right)^{3/2}$$

$$\alpha_{55^+} = 4.6 \times 10^{-6} \left(\frac{300}{T}\right)^{3/2}$$

$$\alpha_{30^+} = 4.0 \times 10^{-7} \left(\frac{300}{T}\right)^{3/2}$$

The altitude variations for these coefficients are shown in Figure 7 based on a temperature model from Champion (1965). Note that the effective recombination coefficients derived from our measurements at $\chi = 28^o$ bracket the values for a mean water cluster mass near 55^+. It is shown in Goldberg and Aikin (1971) that 37^+, 55^+ and heavier ions do indeed predominate below 80 km. This result presents a consistent picture between ionospheric and laboratory measurements for the first time since Aikin et al. (1964) pointed out the necessity for large recombination coefficients to accomodate the rocket measurements of nitric oxide. This indicates validity for the theory put forward by Reid (1970) and Landmark et al. (1970) that faster dissociative recombination will occur if the species of ion is a water cluster ion than if it is 30^+. In order to reconstruct the effective recombination coefficient it is necessary to take into account the proportions of the different species of ions.

CONCLUSION

Three equatorial D region electron and positive ion density profiles have been presented for one day. Evaluation of the possible production sources leads to the conclusion that X-rays, photoionization of NO, and cosmic rays dominate ion production in the D region. X-ray fluxes are determined by rocket-borne proportional counter experiments aboard two of the rockets and are found to concur with the integrated total flux measured aboard the Solrad 9 satellite at that time.

Comparison of the measured electron density profiles with the X-ray flux and recent measurements of nitric oxide provide effective recombination coefficients between 4×10^{-6} cm^3/sec and 1×10^{-5} cm^3/sec in accord with recent measurements of the electron-ion recombination coefficient for heavier hydrated cluster ions near mass 55^+. No additional mechanisms, e.g. large concentration of negative ions, are required to resolve the long-standing discrepancy between ion-pair production rates due to ionization of nitric oxide and laboratory measurements of loss processes.

It was shown by Aikin (1966) that for recombination coefficients as large as 10^{-6} $cm^3 sec^{-1}$, no diurnal asymmetry of electron density is expected. Hence the apparent asymmetry about noon cannot be explained at the present time. A large gradient in electron density above 85 km often observed at midlatitudes is also present at the equator.

ACKNOWLEDGEMENT

This program was successfully completed through the diligent efforts of the technical staff assigned to the Chemosphere Branch for direct support of this work. In particular, we wish to thank Messrs. Roy Hagemeyer, Giles Spaid and Donald Silbert. We also express our appreciation to members of the Goddard Sounding Rocket Division for the many services they performed including introduction of tone ranging to determine trajectory. The assistance of John Jackson in the trajectory analysis is greatly appreciated. Thanks are also due the Indian Launch Range (TERLS) personnel under the directorship of Mr. H.G.S. Murthy, for their excellent cooperation and support.

REFERENCES

Aikin, A.C., 1966, Ground-Based Radio Wave Propagation Studies of the Lower Ionosphere, Conference, Ottawa, Canada.

Aikin, A.C., J.A. Kane and J. Troim, 1964, J. Geophys. Res., 69, 4621-4628.

Barth, C.A., 1966, Ann. Geophys., 22, 198.

Biondi, M.A., private communication.

Bourdeau, R.E., A.C. Aikin and J.L. Donley, 1966, J. Geophys. Res., 71, 727.

Champion, K.S.W., 1964, Air Force Cambridge Research Laboratories Report AFCRL-65-443.

Goldberg, R.A. and A.C. Aikin, 1971, Document X-625-71-73, Goddard Space Flight Center, Greenbelt, Maryland.

Gnanalingam, S., private communication.

Haug, A., E.V. Thrane, E. Tsagakis and M. Anastassiades, 1970, J. Atm. Terr. Phys., 32, 1865.

Hudson, R.D., 1971, paper presented at COSPAR Symposium on D and E Region Ion Chemistry.

Huffman, R.E., D.E. Paulsen, J.C. Larrabee and R.B. Cairns, 1971, J. Geophys. Res., 76, 1028-1038.

Hunten, D.M. and M.B. McElroy, 1968, J. Geophys. Res., 73, 2421.

Inn, C.Y., 1961, Planet. Space Sci., 5, 76-78.

Inn, C.Y., 1961, Planet. Space Sci., 8, 200-201.

Kane, J.A., 1969, GSFC X-615-69-499.

Kreplin, R.W., private communication.

Kreplin, R.W., 1961, Annal. de Geophys., 17, 151-161.

Landmark, B., A. Haug, E.V. Thrane, J.E. Hall, A.P. Willmore, M. Jespersen, B. Moller Pedersen, M. Anaslassiades, E. Tsagakis and J.A. Kane, 1970, J. Atm. Terr. Phys., 32, 1872-1883.

Meira, L.G., Jr., 1971, J. Geophys. Res., 76, 202-212.

Nicolet, M. and A.C. Aikin, 1960, J. Geophys. Res., 65, 1469-1483.

Pearce, J.B., 1969, J. Geophys. Res., 74, 853.

Rao, M.K., S.C. Magundar and S.N. Mitra, 1962, J. Atm. Terr. Phys., 24, 245.

Reid, G.C., 1970, J. Geophys. Res., 75, 2551-2562.

Rusch, D.W. and C.A. Barth, 1971, Paper presented at COSPAR Symposium on D and E Region Ion Chemistry.

Somayajulu, Y.V. and A.C. Aikin, 1969, Paper presented at COSPAR, Leningrad, May 1970. (See also Aeronomy Report 32, 375, University of Illinois).

TABLE LIST

Table 1 - Summary of instrumentation, launch times and solar zenith angles for rockets 14.425, 14.424 and 14.372 An X implies that the experiment was carried aboard the specified payload.

TABLE I

Rocket Number	14.425	14.424	14.372
Solar Zenith Angle	53.2^{o}	27.8^{o}	48.3^{o}
Time of Launch (LMT)	0827	1017	1509
Electron density (radio propagation)	X	X	X
Electron density (nose tip probe)			X
Positive ion density (Gerdien condenser)	X	X	
Positive ion composition (quadrupole ion mass spectrometer)	X	X	
Solar, Lyman α & O_2 density (ion chambers)	X	X	X
Solar X-rays (proportional counter)	X		X

FIGURE CAPTIONS

Figure 1 - Electron and positive ion density altitude distribution; 1a-14.425, 1b-14.424, 1c-14.372.

Figure 2 - Gerdien condenser for measuring positive ion number density.

Figure 3 - Comparison of electron density profiles for March 19, 1970 at Thumba, India.

Figure 4 - X-ray spectra obtained from 14.424 and 14.372. Gray body curves are described in the text.

Figure 5 - Comparison of nitric oxide distributions adapted from Meira (1971). Arrow on Barth's curve refers to correction required for Rayleigh scattering.

Figure 6 - D region production function for a solar zenith angle of 28^{o}.

Figure 7 - Effective recombination coefficient profiles derived from 14.424. Upper and lower limit curves refer to limits on Meira (1971) data. Shown for comparison are the dissociative recombination coefficients of H_3O^+, $H_3O^+ \cdot H_2O$, and $H_3O^+ \cdot (H_2O)_2$.

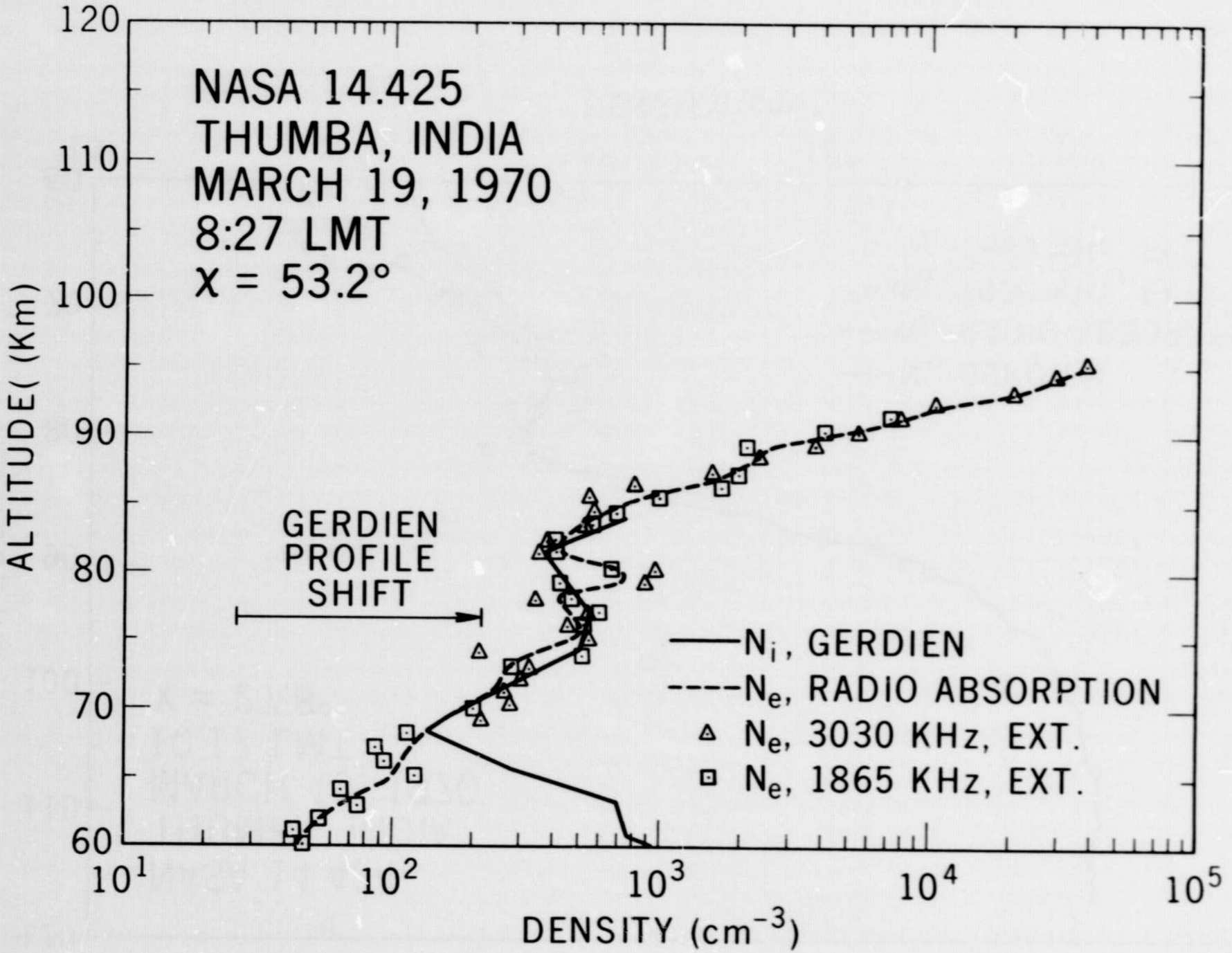
NASA 14.425
THUMBA, INDIA
MARCH 19, 1970
8:27 LMT
χ = 53.2°
GERDIEN
PROFILE
SHIFT
N_i, GERDIEN
N_e, RADIO ABSORPTION
N_e, 3030 KHz, EXT.
N_e, 1865 KHz, EXT.
ALTITUDE((Km)
DENSITY (cm^{-3})
120
110
100
90
80
70
60
10^1
10^2
10^3
10^4
10^5

Figure 1a

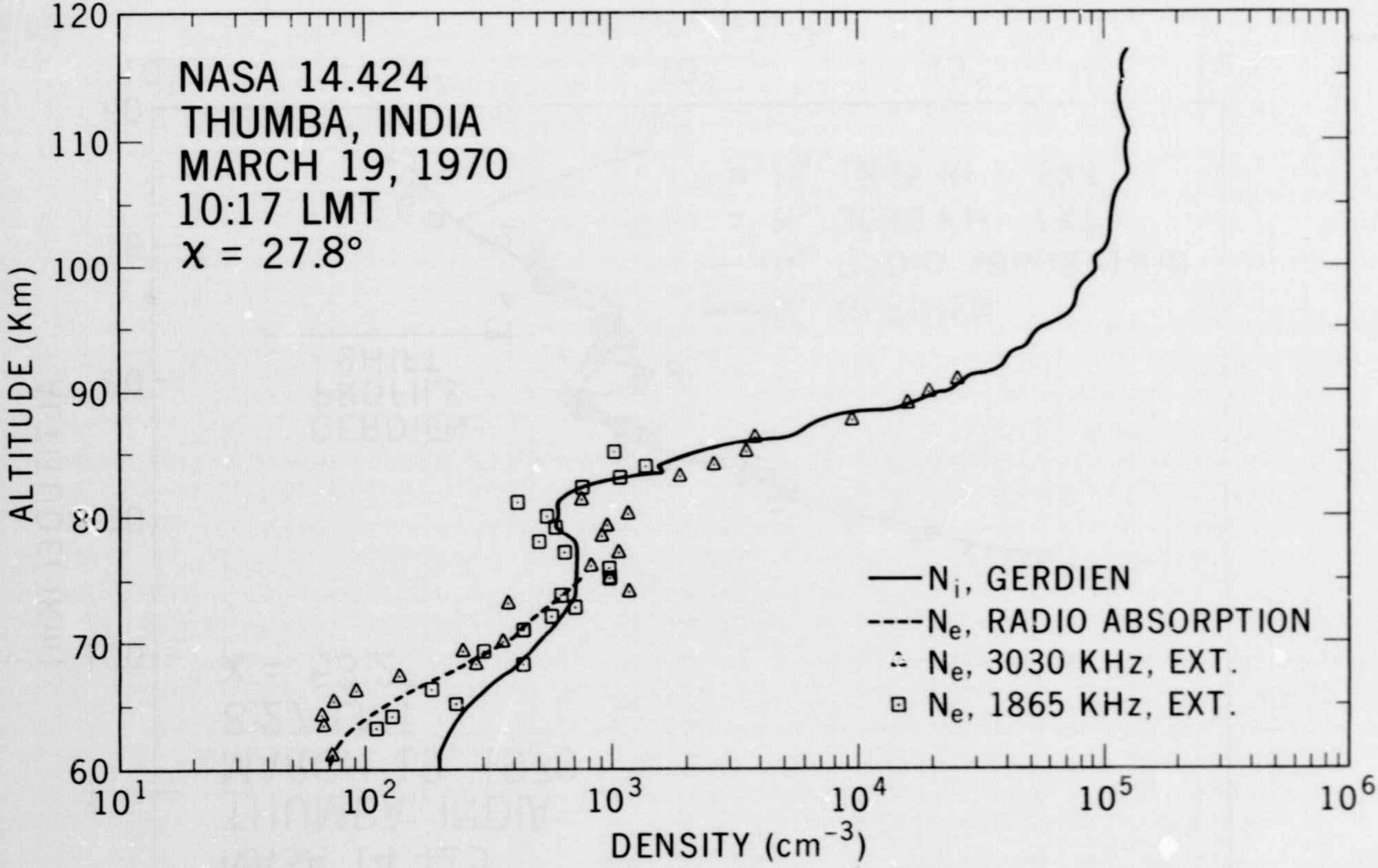
NASA 14.424
THUMBA, INDIA
MARCH 19, 1970
10:17 LMT
χ = 27.8°
ALTITUDE (Km)
DENSITY (cm⁻³)
120
110
100
90
80
70
60
10¹
10²
10³
10⁴
10⁵
10⁶
Nᵢ, GERDIEN
Nₑ, RADIO ABSORPTION
Nₑ, 3030 KHz, EXT.
Nₑ, 1865 KHz, EXT.

Figure 1b

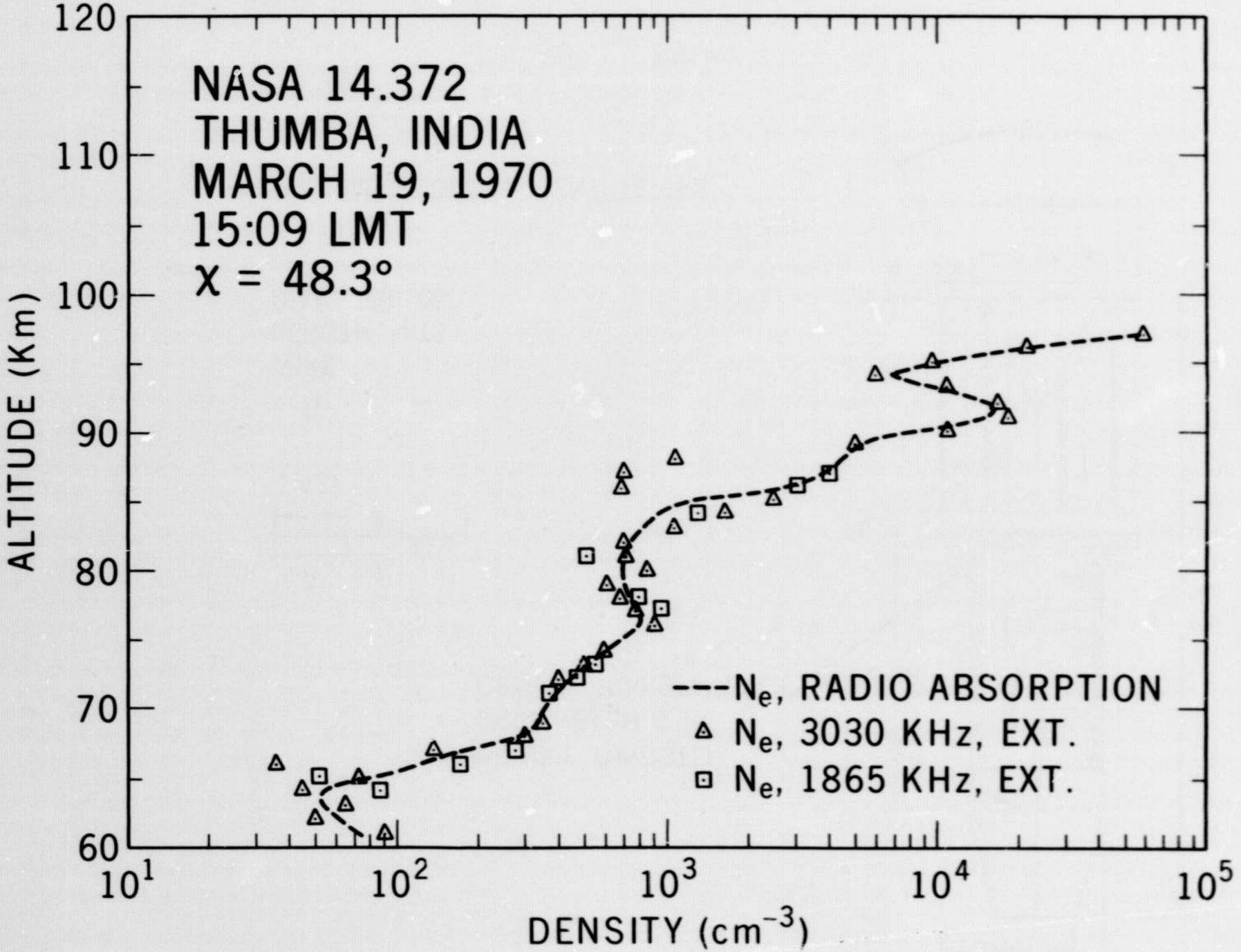
NASA 14.372
THUMBA, INDIA
MARCH 19, 1970
15:09 LMT
χ = 48.3°
ALTITUDE (Km)
120
110
100
90
80
70
60
10^1
10^2
10^3
10^4
10^5
DENSITY (cm^{-3})
---N_e, RADIO ABSORPTION
△ N_e, 3030 KHz, EXT.
□ N_e, 1865 KHz, EXT.

Figure 1c

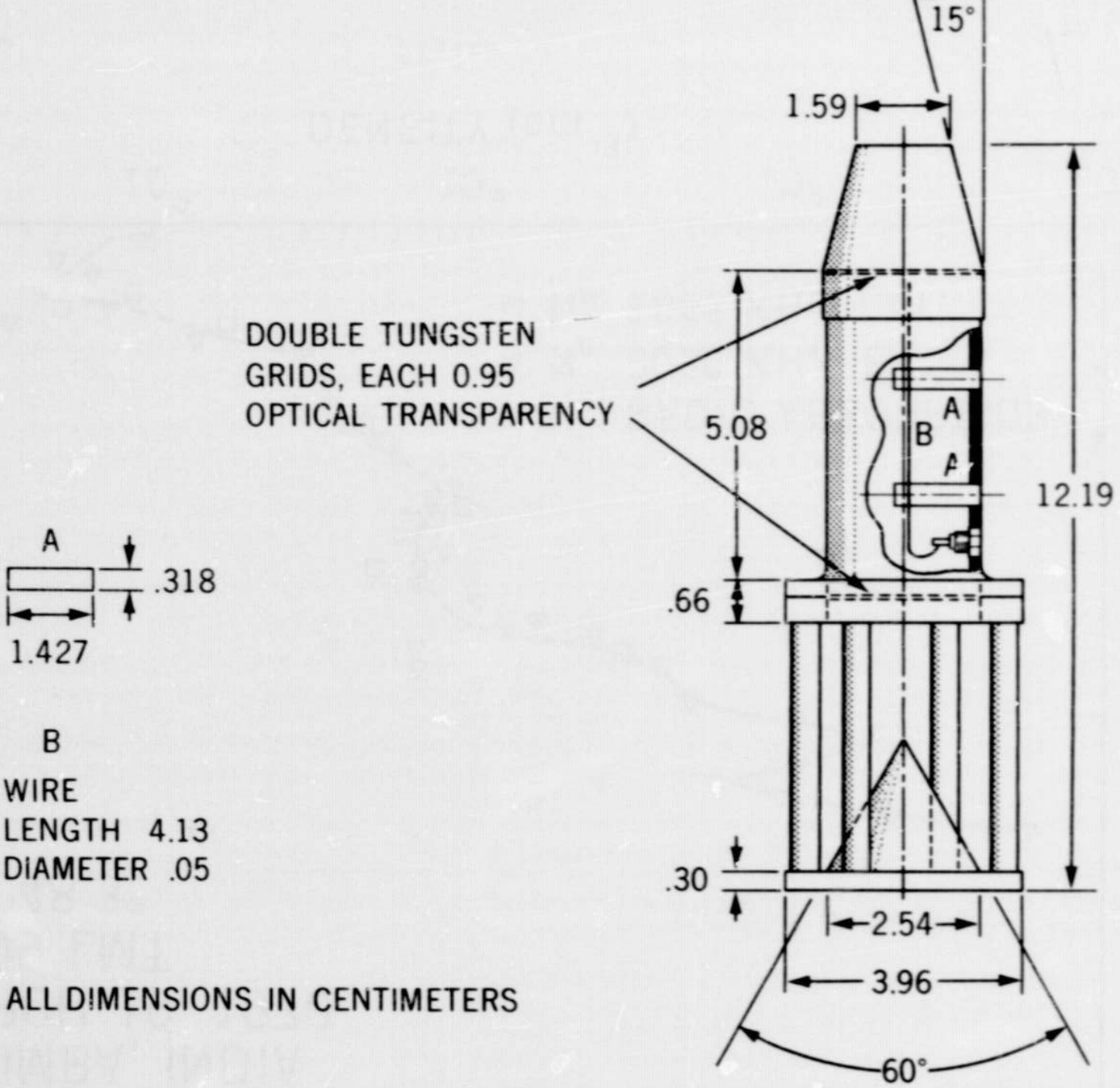
15°
1.59
DOUBLE TUNGSTEN
GRIDS, EACH 0.95
OPTICAL TRANSPARENCY
5.08
A
B
12.19
A
.318
1.427
.66
B
WIRE
LENGTH 4.13
DIAMETER .05
.30
2.54
3.96
60°
ALL DIMENSIONS IN CENTIMETERS

Figure 2

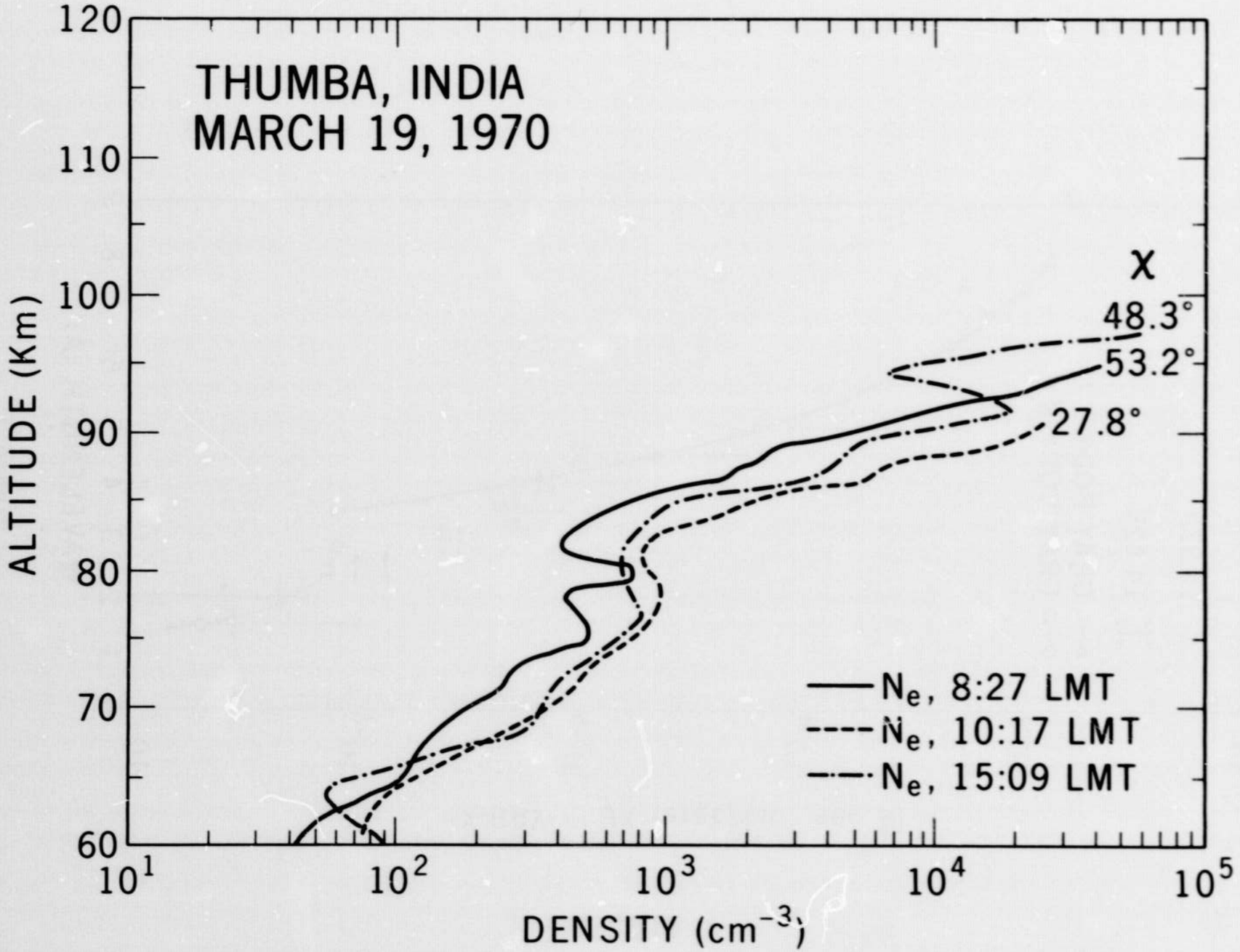
THUMBA, INDIA
MARCH 19, 1970
ALTITUDE (Km)
DENSITY (cm^{-3})
120
110
100
90
80
70
60
10^1
10^2
10^3
10^4
10^5
χ
48.3°
53.2°
27.8°
N_e, 8:27 LMT
N_e, 10:17 LMT
N_e, 15:09 LMT

Figure 3

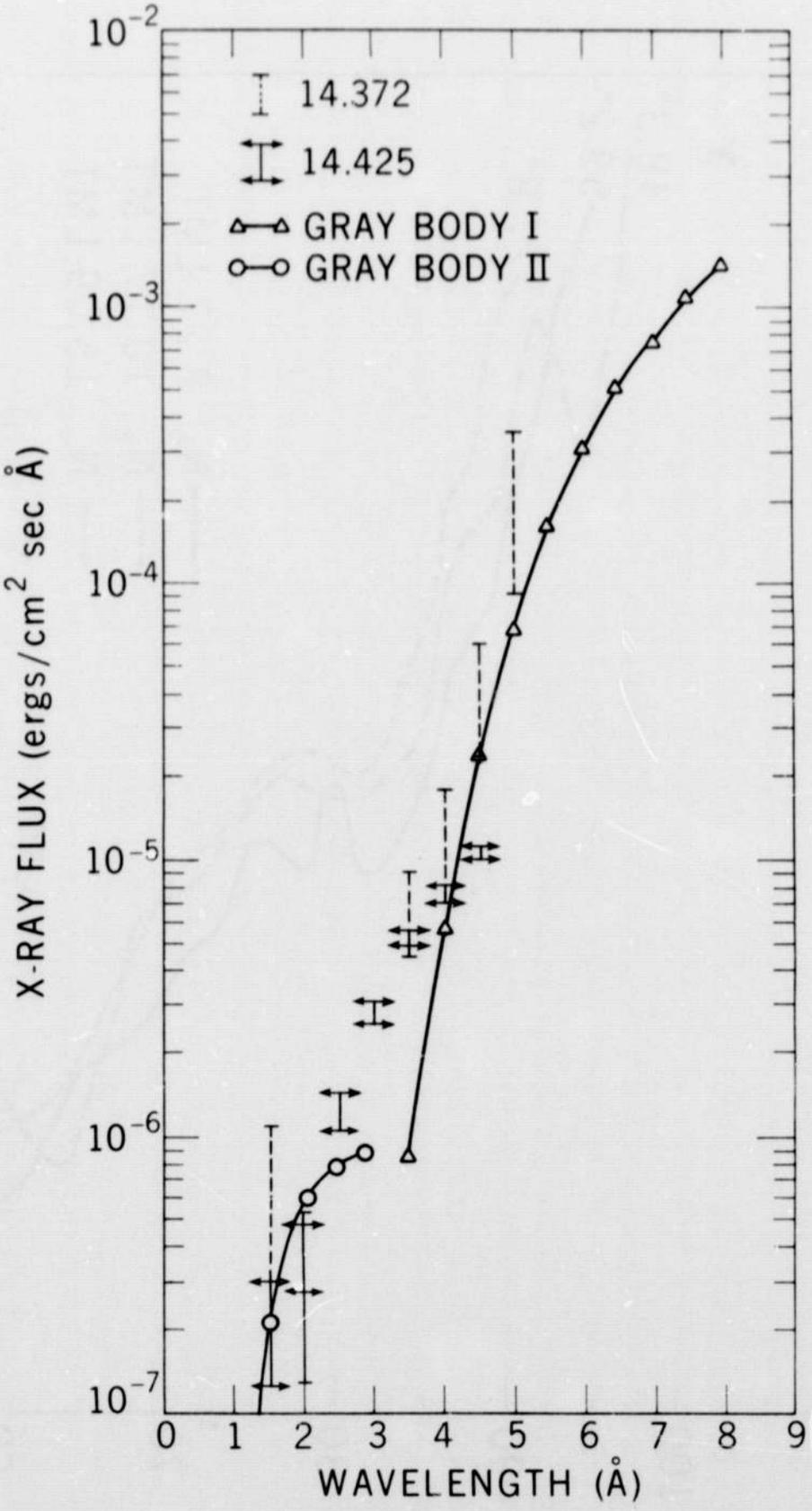
14.372
14.425
GRAY BODY I
GRAY BODY II
X-RAY FLUX (ergs/cm^2 sec Å)
WAVELENGTH (Å)
10^{-2}
10^{-3}
10^{-4}
10^{-5}
10^{-6}
10^{-7}
0 1 2 3 4 5 6 7 8 9

Figure 4

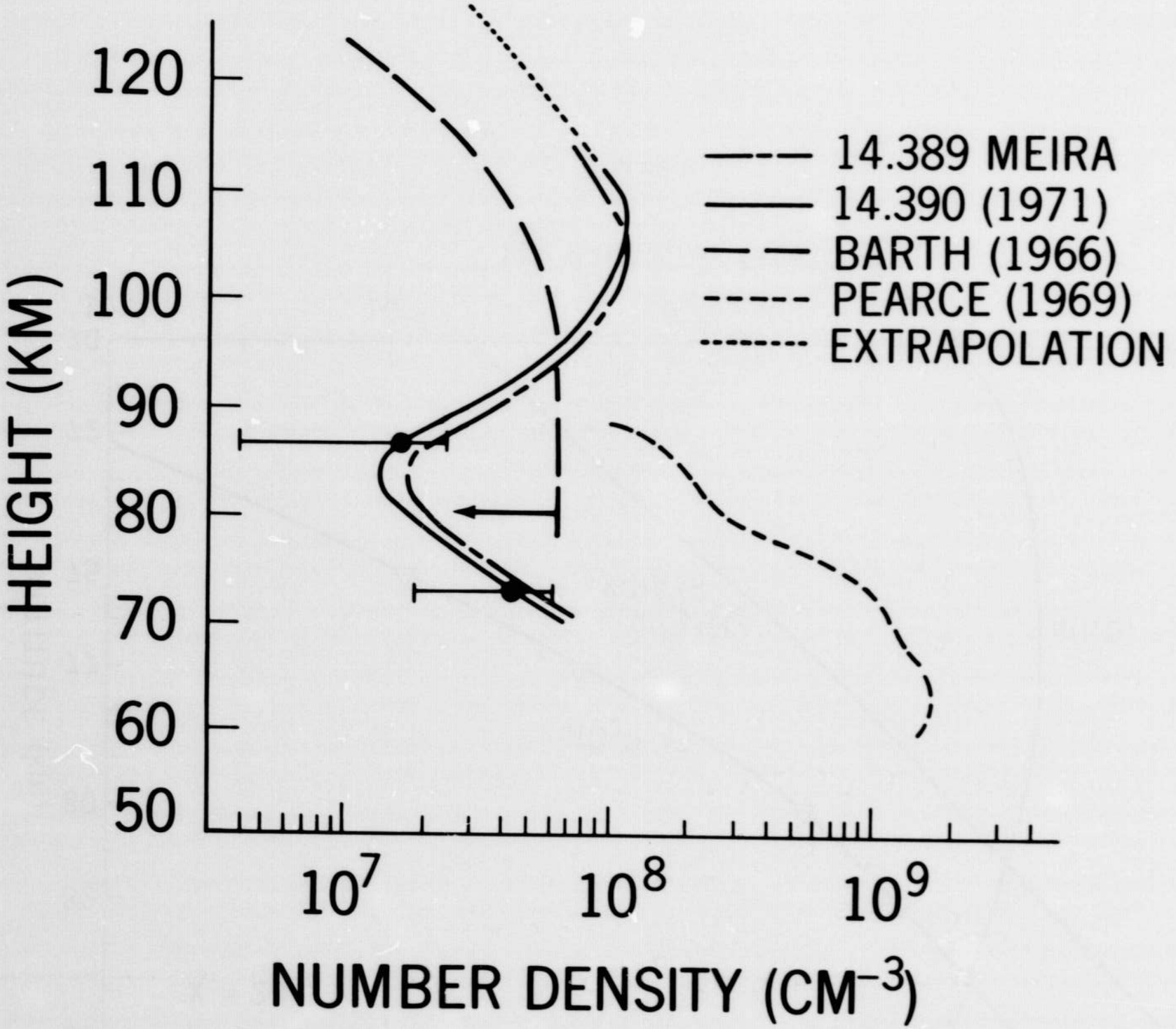
120
110
100
90
80
70
60
50
HEIGHT (KM)
14.389 MEIRA
14.390 (1971)
BARTH (1966)
PEARCE (1969)
EXTRAPOLATION
10^7
10^8
10^9
NUMBER DENSITY (CM^{-3})

Figure 5

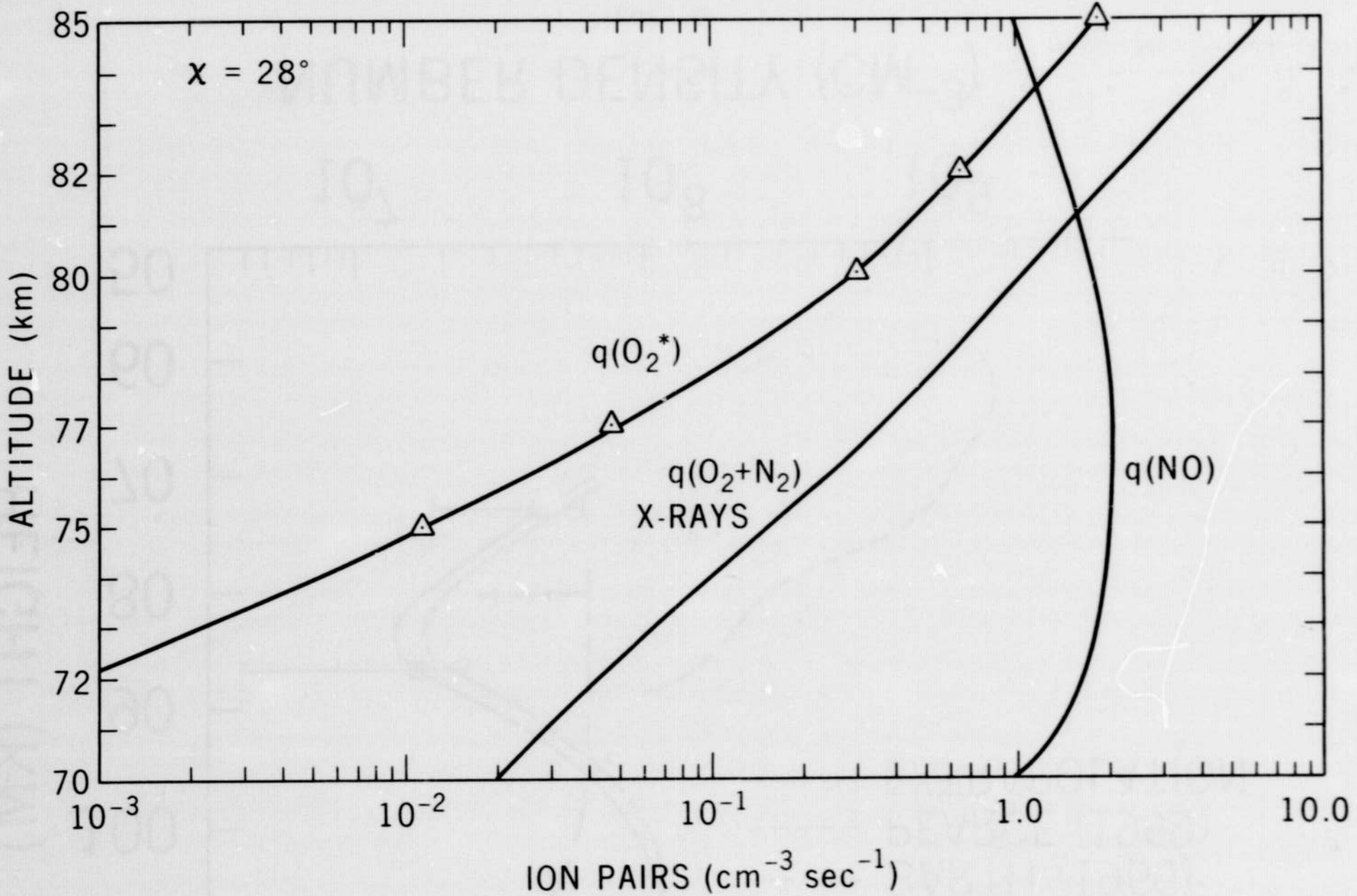
χ = 28°
ALTITUDE (km)
85
82
80
77
75
72
70
10^{-3}
10^{-2}
10^{-1}
1.0
10.0
ION PAIRS (cm^{-3} sec^{-1})
$q(O_2^*)$
$q(O_2+N_2)$
X-RAYS
q(NO)

Figure 6

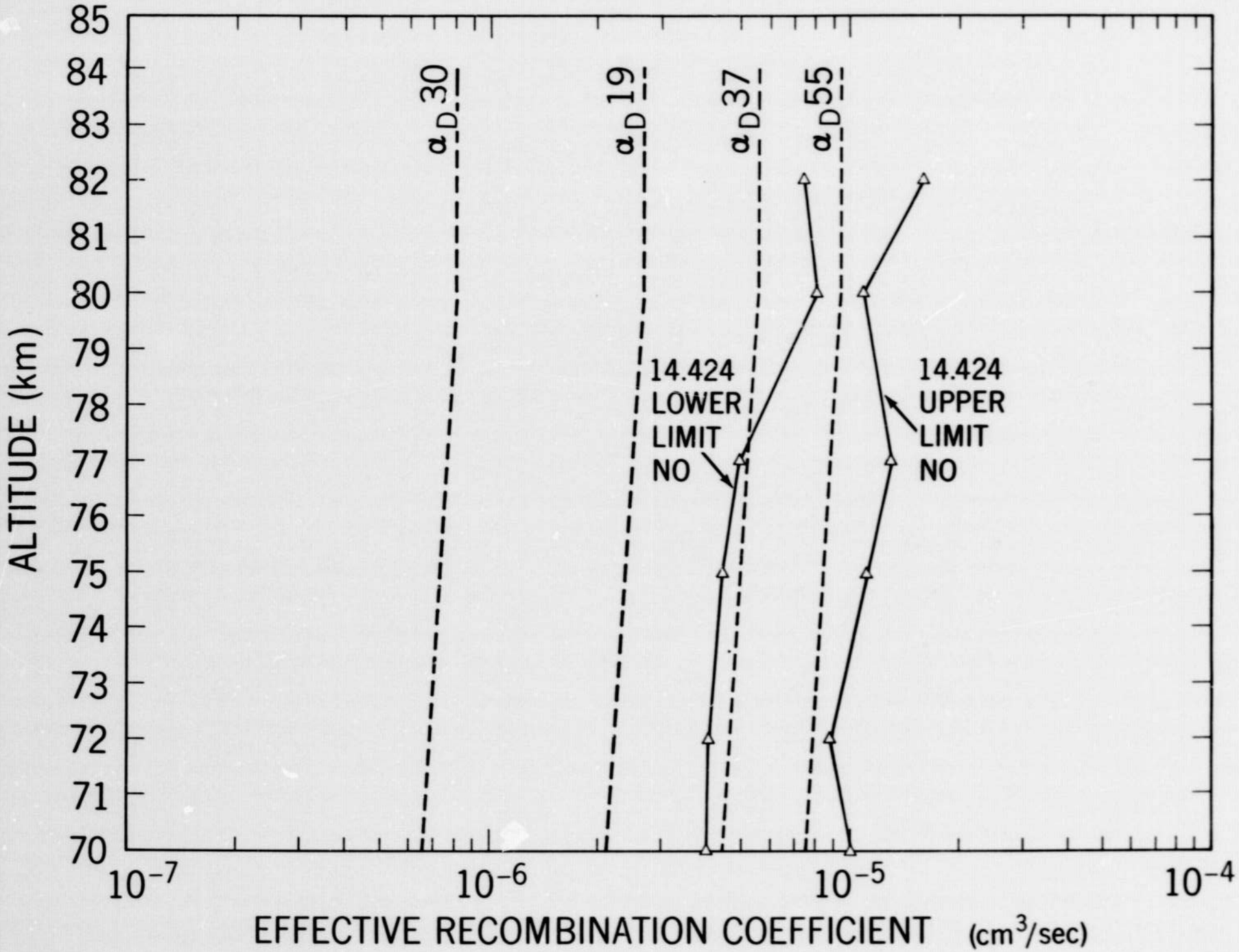
85
84
83
82
81
80
79
78
77
76
75
74
73
72
71
70
ALTITUDE (km)
α_D30
α_D19
α_D37
α_D55
14.424
LOWER
LIMIT
NO
14.424
UPPER
LIMIT
NO
10^{-7}
10^{-6}
10^{-5}
10^{-4}
EFFECTIVE RECOMBINATION COEFFICIENT (cm^3/sec)

Figure 7